Absolute quantification in SPECT

**Philipp Ritt · Hans Vija · Joachim Hornegger ·
Torsten Kuwert**

Abstract Single-photon emission computed tomography
(SPECT) allows the three-dimensional visualization of
radioactivity within the human body and is widely used
for clinical purposes. In SPECT, image quality is compro-
mised by several factors including photon attenuation,
photon scatter, the partial volume effect, and motion
artefacts. These variables also confound the capacity of
SPECT to quantify the concentration of radioactivity within
given volumes of interest in absolute units, e.g. as
kilobecquerels per cubic centimetre. In the last decade,
considerable technical progress has been achieved in
SPECT image reconstruction, involving, in particular, the
development of iterative image reconstruction techniques.
Furthermore, hybrid cameras integrating a SPECT camera
with an X-ray CT scanner have become commercially
available. These systems allow the acquisition of SPECT
and CT datasets registered to each other with a high
anatomical accuracy. First studies have shown that iterative
SPECT image reconstruction techniques incorporating
information from SPECT/CT image datasets greatly in-
crease the accuracy of SPECT in quantifying radioactivity
concentrations in phantoms and also in humans. This new
potential of SPECT may improve not only diagnostic
accuracy, but also dosimetry for internal radiotherapy.

Keywords SPECT · SPECT/CT · Hybrid imaging ·
Dosimetry · Quantification · Absolute quantification

P. Ritt (✉) · T. Kuwert
Clinic of Nuclear Medicine,
Friedrich-Alexander-Universität Erlangen-Nürnberg,
Krankenhausstr. 12,
91054 Erlangen, Germany
e-mail: philipp.ritt@uk-erlangen.de

H. Vija
Siemens Medical Solutions,
Hoffman Estates, IL, USA

J. Hornegger
Department of Pattern Recognition,
Friedrich-Alexander-Universität Erlangen-Nürnberg,
Erlangen, Germany

Introduction

Single-photon emission computed tomography (SPECT)
and positron emission tomography (PET) allow the visual-
ization of the distribution of radioactivity within the human
body. Both modalities are widely used for clinical purposes
(for reviews, see for example Bockisch et al. [1], von
Schulthess et al. [2]). SPECT and PET also hold the
promise to exactly quantify the concentration of radioac-
tivity within a given volume of tissue in absolute units, e.g.
as kilobecquerels per cubic centimetre. This process is
compromised by photon scatter [3–5], photon attenuation
[6–9], and partial volume artefacts [10, 11]. In PET, options
to correct for these confounding variables were developed
and validated several decades ago (for reviews, see for
example Schelbert et al. [12], Boellaard et al. [13]) owing
to the technical advantages offered by positron decay and
coincidence detection. In SPECT, technical progress in that
regard has been considerably slower with various reports
emphasizing the lack of quantitative ability [14–16].

In the present article, we review recent progress in that
field for SPECT. For orientation, a simplified diagram of
the image formation chain for quantitative SPECT is given
(Fig. 1). We start our review with the reconstruction that
nowadays incorporates many correction methods men-
tioned in the later paragraphs. We then focus on attenuation,
scatter, and partial volume effects. In each of the paragraphs

Fig. 1 Illustration of a simplified image formation chain. The image of the true activity distribution is confounded by several effects, including attenuation, scatter, partial volume, and motion. The SPECT reconstruction, along with corrections for the mentioned effects, delivers a measured, three-dimensional count distribution. With a calibration step, the count distribution is translated into a measured activity distribution
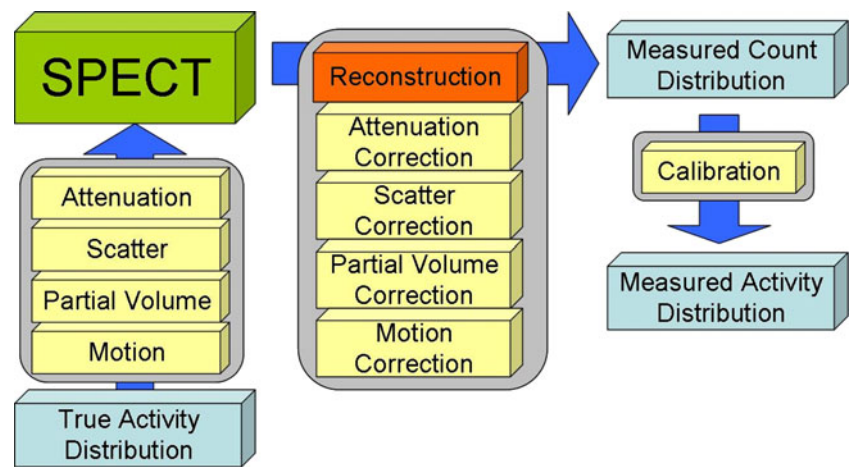
a short explanation of the underlying effect and an overview of correction techniques are given. In addition, we briefly outline a calibration technique. We conclude with a discussion of the potential of SPECT quantification for clinical applications and present some validation studies.

In general, we assume in the following that the kinetics of the activity distribution that is of interest are slow with respect to the imaging time. If this is not the case, significant quantification errors could occur and other approaches such as dynamic SPECT may be beneficial [17].

Quantitative reconstruction

In general, two main families of reconstruction techniques are commonly used in clinical emission CT: non-iterative (e.g. filtered back-projection, FBP) and iterative methods. Despite its higher demands on computation, iterative reconstruction seems to be superior for quantification than non-iterative methods. In principle this is mainly due to the ability to implement corrections and system modelling methods more readily in iterative reconstruction than in non-iterative methods. Consequently, several publications have reported higher quantitative accuracy of iterative reconstructions than of non-iterative methods [18–20].

In the following the most important parts of the system modelling are explained (Fig. 2). In general, the application of such models in reconstruction leads to improved system resolution and quantitative accuracy.

As an example, one assumption of the FBP algorithm is that the sensitive volume of one collimator hole is of cylindrical shape. However, in reality, the sensitive volume is more cone-shaped. As a result, the system resolution, defined as full-width at half-maximum (FWHM) of a point source, depends approximately linearly on the distance between the source and detector for a gamma camera that

employs absorptive parallel-hole collimation. This effect, known as the geometric response function, can easily be incorporated as a mathematical model into an iterative reconstruction—in contrast to FBP.

The intrinsic effects of the detector are characterized by the intrinsic response function. This function mainly
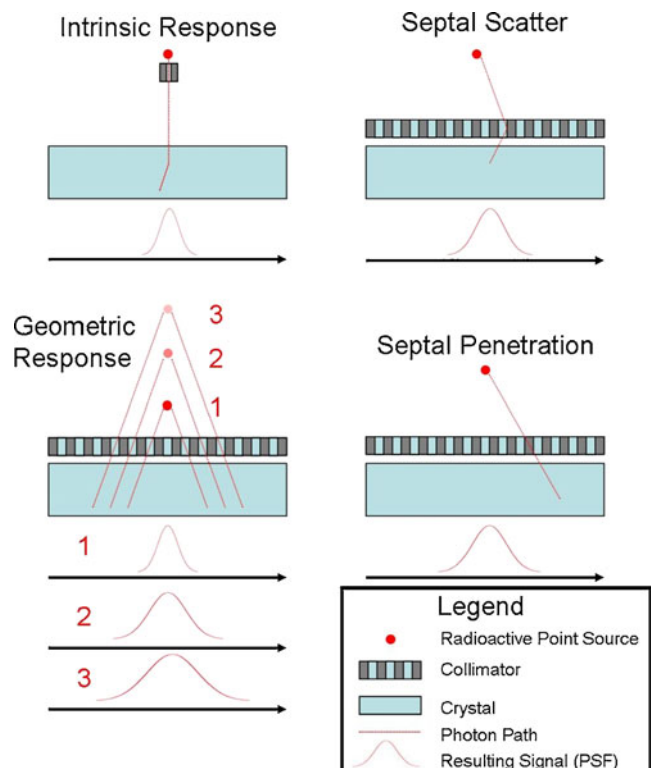

Fig. 2 Simplified illustration of some components that form the collimator–detector response function. The geometric response function (*lower left*) models source-to-collimator distance effects (the measured response in the crystal varies with source-to-collimator distance). The intrinsic response function (*upper left*) describes the effects of interactions in the detector crystal itself (the point source is collimated to form a pencil beam). The septal scatter function (*upper right*) and septal penetration function (*lower right*) model the interactions between gamma radiation and the collimator

describes the effect of scatter in the crystal itself and the uncertainty in the position estimation of a detected photon.

In SPECT imaging a compromise between collimator efficiency and image quality has to be made. Thicker collimator septa reduce the amount of septal penetration; however, they also reduce the efficiency of the collimator by covering the sensitive area of the detector. As a result of the compromise made, a certain amount of septal penetration is allowed (e.g. 5%). In general the probability that photons penetrate the septa of the collimator is described by a septal penetration function, and this can be incorporated to correct for the effect.

Another possible interaction between the photons and collimator septa is scatter. The probability that photons are scattered by the septa is modelled by the septal scatter function; this is in general more important for medium and high-energy nuclides.

The combination of the four parts of the response function (see Fig. 3) is known as the collimator–detector response function. It is used to correct for the effects described above in the reconstruction step and consequently helps to improve system resolution and quantitative accuracy.

Analytical corrections for the response functions that can be implemented in non-iterative techniques are possible. However, there are several studies that have shown that superior resolution and improved quantitative accuracy can be achieved when corrections are implemented using iterative reconstruction techniques [21–23]. For example, Römer et al. [8] have reported the use of a three-dimensional depth-dependent blur modelling (OS-EM 3D reconstruction) in a clinical environment. A more detailed review of the modelling of the collimator–detector response function is beyond the scope of this article, but can be found in reference [24].

For clinical SPECT quantification, iterative reconstruction is the state of the art and is in general recommended. Corrections for the geometric response and the intrinsic response are thought to be more important than the modelling of septal scatter and penetration (at least for low-energy imaging) and if available, should be applied. The improved spatial resolution will significantly decrease the confounding effect of partial volume and will thus result in higher quantitative accuracy in the imaging of small structures.

Attenuation correction

SPECT images are grossly affected by attenuation artefacts. In the case of SPECT imaging the probability P_{Det} that a gamma quantum emitted at d reaches the detector at position D (assuming that it is emitted in the proper direction) is calculated according to Eq. 1 (see Fig. 4 for a simplified illustration):

$$P_{\text{Det}} = \exp\left\{ \int_{\vec{d}}^{\vec{D}} -\mu(\vec{r})d\vec{r} \right\} \qquad (1)$$

The integral covers essentially the path of the radiation from its origin through the object, to the location of detection.

The probability of detection in SPECT consequently depends on the (unknown) location of the decay d and on the linear attenuation coefficients $\mu(r)$ of the object. In contrast, in PET imaging the probability only depends on the line of response (LOR) where the decay happened, and not on the exact location in this LOR. For the correction of the attenuation effect in the reconstruction step, the spatial distribution of the attenuation coefficients of the examined object for the photon energy of the radionuclide used needs to be known. Several methods for obtaining attenuation maps have been employed. The maps can be estimated, if the contours of the object (e.g. via rough segmentation of the SPECT image) and the attenuation coefficients are known (e.g. attenuation coefficient of water). The object can be assumed to be homogeneous with regard to this coefficient (Chang's correction [25]). This method is still very successfully applied to SPECT imaging of the brain, where one class (soft brain tissue) predominates. However, it is not very accurate for SPECT imaging of the thorax and pelvis, where large amount of other tissues (e.g. lung and bone) are present. Another way of generating the attenuation maps is through a simple transformation of a transmission scan. The transmission images need to be converted to attenuation factors at the effective energy of the emission scan (140 keV for ^{99m}Tc), and corrected for the spatial registration between the emission and transmission images. The resulting attenuation map can be easily integrated into common iterative reconstruction techniques for SPECT images.

Before the introduction of hybrid SPECT/CT devices, radionuclide (source-based) transmission measurements (e.g. ^{153}Gd, ^{99m}Tc, ^{133}Ba) were commonly employed. These source-based methods have the advantage that the same detector can be used for both the emission and the transmission scans, which makes the methods very cost-efficient. However, these detectors are disadvantageous for the image quality of the transmission scan, due to a poor signal-to-noise ratio and due to a limited spatial resolution. Furthermore, due to radiation safety considerations, only relatively weak transmission sources are used, which result in lengthy transmission scans, lasting 10 min and more, with further limitations to count statistics. Poor tissue contrast at

Fig. 3 The combination of models for the intrinsic response and geometric response, and for septal scatter and septal penetration is called the collimator–detector response function. It can be integrated into the (iterative) reconstruction step

Components of Collimator-Detector Response Function
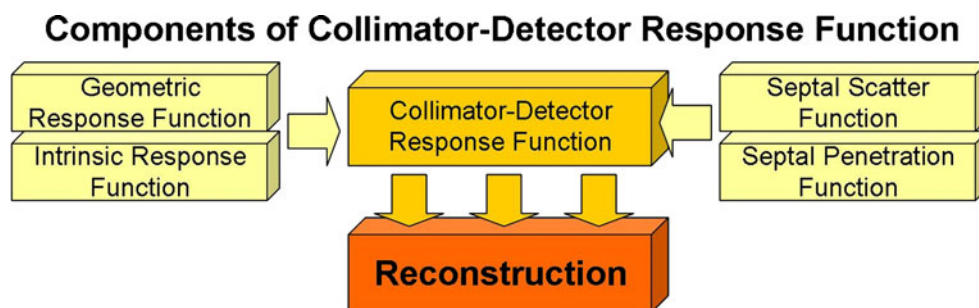
the relatively high photon energies of the transmission source (100–400 keV) limits the effectiveness of these images for image fusion even further compared to effective photon energies of an X-ray CT (40–90 keV).

With the advent of hybrid SPECT/CT, and thus the availability of highly correlated high-quality X-ray CT transmission scans, it is now standard to use these scans not only for fused viewing, but also for attenuation correction. The CT scans, usually in Hounsfield units, have to be converted to linear attenuation coefficients at the respective photon energy. It is important to note that the transformation of the CT transmission image to attenuation factors at the effective energy of the emission scan can introduce errors [26]. First, the transformation is specific for different acceleration voltages and beam filters of the CT scanner. Second, the polychromaticity of the X-ray beam also introduces artefacts, mainly caused by beam hardening. Patient motion that occurs between the emission and transmission acquisitions in a hybrid system can lead to artefacts, which in turn can lead to false readings of the SPECT images. Manual post-registration could help to prevent such artefacts [27].

Attenuation correction is obligatory for accurate SPECT quantification. Methods that rely on the segmentation of contours in SPECT are sufficient for SPECT quantification in "easy" anatomies such as the brain. However, attenuation correction by SPECT/CT seems to have become the clinical standard and is highly recommended for quantification.

Scatter correction

In another assumption implied by the simple reconstruction used in "early" SPECT, crosstalk between the individual lines of response of a collimator was neglected. This assumption fails if photon scatter occurs (which necessarily is always the case). Scatter correction is another important requirement for (quantitative) SPECT imaging. Scattered radiation is produced when gamma quanta emitted from decaying nuclei interact with surrounding atoms. Compton scattering is the prevalent scatter process in the energy range of clinically utilized radiotracers.

The energy E_S of the scattered photon depends only on the scattering angle ϕ and is given by Eq. 2, where E_0 is the energy of the photon before scattering and $m_e c^2$ the invariant mass of the electron. The energy transfer thus does not depend on the density or atomic number of the absorbing material. However, the total probability that a photon is scattered by this effect depends heavily on the properties of the absorbing material, most importantly electron density.

As seen in Eq. 2, the gamma quanta lose energy and change their momentum and direction in the scatter process. Because of the intrinsic energy resolution of the detector, the system cannot discriminate between unscattered quanta and quanta that have lost a small amount of energy in the scatter process. As a consequence some scatter is allowed into the image formation.

$$E_s = E_0 / \left[1 + \left(E_0 / m_e c^2 \right) \cdot (1 - \cos(\varphi)) \right] \tag{2}$$

Fig. 4 Simplified illustration for the detection of a decay event. The signal from the decay at position d is decreased by attenuation effects. The amount of attenuation depends on the (spatially varying) linear attenuation coefficients $\mu(x,y,z)$ and on the distance between the detector and the decay, namely on $|D-d|$

In simple FBP with parallel-hole collimation, it is assumed that the decay takes place exactly perpendicular to the detection plane and detection location. For the detected scatter quanta, because of the change in direction, not only the distance between the decay and the location of detection along the LOR is unknown, but also the correct position of the LOR itself. However, not all information about the originating nuclei is lost. Scattered radiation is therefore often understood as anisotropic noise that reduces the quality of the SPECT image.

There are a variety of methods to correct for scattered radiation. Some of them are "passive" methods: For example, the photopeak energy window could be narrowed or the lower discriminator cut-off of the window could be increased in order to avoid accepting scattered photons. Koral et al. [28] reported improved quantitative accuracy with this technique. A significant drawback of this method is that unscattered photons are also rejected due to the limited energy resolution of the gamma camera. Even with a relatively small energy window of ±5 keV for ^{99m}Tc (140 keV), on the basis of Eq. 2, photons with scatter angles of up to 30° are still accepted. More common approaches utilize dual [3], triple [29] and even multiple [4] energy windows. The additional scatter energy windows are placed below or above the photopeak energy window; the scatter images are acquired simultaneously with the photo-peak image. For each pixel of the projection image, the amount of scattered radiation in the photopeak window image is estimated from the scatter window images. Subsequently this amount can be subtracted from the projections or incorporated into the iterative reconstruction.

Besides the simple multiple energy window approach, there are a multitude of other approaches for estimating and correcting for scattered radiation (for an overview see reference [30]). Despite the diversity in the methods employed, many reports stress the importance of accurate scatter correction for quantitative SPECT. Shcherbinin et al. [31] and Vandervoort et al. [32] incorporated a method based on the work of Wells et al. [33] in their iterative reconstruction forward projection step that utilizes the Klein-Nishina formula, and reported an improved quantitative accuracy in phantoms measurements. Monte-Carlo methods seem to promise even more accurate results [34–36]. However, their application in clinical practice is still limited due to the high computational costs and patient specificity.

Many scatter correction techniques are available; unfortunately, only very few are applicable in a clinical environment. Despite their simplicity, dual or multiple energy window approaches can be recommended due to their ability to correct for scattered radiation and their ease of application. The results from the scientific literature (see Validation studies) for in vivo quantification support this recommen-dation. The superiority and applicability of the more sophisticated techniques in daily clinical usage still have to be proven.

Partial volume correction

Partial volume effects are caused by the limited spatial resolution of emission tomography devices. Regions of interest (ROIs) in structures with heterogeneous activity distribution below approximately twice the FWHM of the spatial resolution are degraded: Their activity is either under- or over-estimated, depending on the combination of "spill-in" and "spill-out" effects. Spill-in refers to the effect that activity from outside the ROI or structure due to the limited spatial resolution is integrated into the ROI: The activity inside the ROI is increased. Spill-out is understood as the activity of the ROI/structure is distributed over the borders (again due to the limited spatial resolution) and therefore "lost" for the quantification of that structure: The activity inside the ROI is decreased. The degree of the partial volume effect depends on the (spatially varying) system resolution of the imaging system, the patient (e.g. motion), and the true distribution of radioactivity in the image.

In SPECT systems, the image spatial resolution (which, in the following, is understood as the FWHM of a point source) is limited mainly by collimator performance. Unlike PET, SPECT utilizes absorptive collimation to identify the direction of the photon LOR. Only a small fraction of the gamma quanta that hit the collimator surface pass through it. This leads to heavily limited detection efficiency when compared to PET systems (see for example Cherry et al. [37] p. 340). Since there is a trade-off between spatial resolution and detection efficiency, SPECT collimators are typically designed with the maximum allowable resolution in order to partially compensate for the limited detection efficiency.

Besides the collimator design and geometry, the achievable spatial resolution is also influenced by the intrinsic resolution of the detector (the spatial resolution of the detector itself, without a collimator). Today, most SPECT detectors are made of a single crystal plate of NaI that illuminates an array of photomultipliers. The intrinsic resolution of the detector is influenced by the photopeak energy of the imaged radionuclide and the crystal thickness. Higher gamma quantum energy leads to better intrinsic resolution (due to a higher scintillation light output). A thicker crystal increases the intrinsic resolution (due to the broader spread of the scintillation light before it can exit the crystal).

Clinical SPECT detectors typically provide an intrinsic spatial resolution in the range 3–5 mm for ^{99m}Tc. However, the image resolution for the SPECT system depends highly

on the collimator design and the source-to-collimator distance. For parallel-hole collimation of ^{99m}Tc and typical source-to-collimator distances, it commonly ranges from 7 to 15 mm FWHM, which is considerably lower (higher FWHM) than that seen in PET (2–5 mm FWHM). By applying other collimator geometries, e.g. (multi)pinhole, even higher spatial resolution (lower FWHM) than in PET can be achieved [38]. Branderhorst et al. [39] report submillimetre (FWHM) resolution for their small-animal SPECT camera using ^{99m}Tc. However, these collimator geometries still seem to be used more frequently for small-animal studies than in clinical practice. A more detailed description of collimator geometries can be found in reference [37].

Approaches to partial volume correction can be divided into two groups: those that need additional information (e.g. CT, MRI) on the structures that are imaged, and those that work solely on the emission images. (In the following, the ratio of apparent activity concentration to true activity concentration is called recovery coefficient.) A simple to achieve and thus common post-reconstruction approach in the latter group is founded in experiments with physical phantoms, simulation studies or theoretical derivations. Based on the approaches of Hoffman et al. [40] and Kessler et al. [10], recovery coefficients for simple geometries (e.g. spheres, discs, cylinders) can be estimated and consequently can be used to calculate the true amount of radioactivity in such structures. Several groups have reported improved quantification accuracy using this approach [7, 11, 41]. A known limitation of this method is the sole applicability to simple geometries; in general, the distribution of the radioactivity might not follow this assumption. Seo et al. [42] have reported an accuracy of 10% for ^{111}In with their implementation of a deconvolution-based partial volume correction in lesions with a volume down to 8 ml.

All approaches that finally lead to an improved spatial resolution of the imaging system help avoid partial volume effects. Thus, for example, the methods described in the section Quantitative reconstruction which incorporate information about the system's collimator–detector response function could, to some extent, be understood as a partial volume correction technique. For example, Hutton and Lau [43] implemented their version of detector–response modelling in the ML-EM and OS-EM reconstruction and found improved accuracy for the simulated MCAT phantom.

The other group of methods incorporate structural information in the form of segmented MR or CT images in the partial volume correction step. The segmentation can be fully automatic or manual by the definition of ROIs. Pretorius and King [44] applied a method based on the work of Da Silva et al. [45] and Tang et al. [46] that incorporates multiple two-class segmentations (regions with activity and regions without activity) of coregistered

myocardial CT images on the MCAT phantom. They reported improved visual characteristics as well as a higher quantitative accuracy of the corrected SPECT data.

$$
\begin{bmatrix} t_1 \\ t_2 \\ \vdots \\ t_n \end{bmatrix} = \begin{bmatrix} \omega_{11} & \omega_{21} & \cdots & \omega_{n1} \\ \omega_{12} & \ddots & & \omega_{n2} \\ \vdots & & \ddots & \vdots \\ \omega_{1n} & \omega_{2n} & \cdots & \omega_{nn} \end{bmatrix} \times \begin{bmatrix} T_1 \\ T_2 \\ \vdots \\ T_n \end{bmatrix} \quad (3)
$$

An evolution of the above approach is the geometric transfer matrix (GTM) method first applied by Rousset et al. [47, 48] in brain PET studies. It allows an almost arbitrary number of regions (n) with homogeneous activity distribution. The observed activity t_i of a certain tissue class i is assumed to be a linear combination of the true activities T_j of all other tissues classes $j=1\ldots n$. The spatial definition of the regions is commonly done on segmented CT or MRI images. The ω_{ij} represent the regional transfer coefficients: The diagonal terms represent the spill-out of every region; the off-diagonal terms define the spill-in of other regions. The ω_{ij} can be computed from the defined regions and the point spread function of the imaging system. In the end one should get a full-rank transfer matrix. The true activities T_j can be computed by solving the linear equation defined in Eq. 3.

Du et al. [49] compared variants of the GTM approach to uncorrected images in a physical brain phantom filled with ^{99m}Tc and found a strong reduction in the bias induced by a partial volume effect. Soret et al. [50] studied the effect of the GTM approach on ^{123}I again using a physical brain phantom and segmented CT acquisitions. For uncorrected images and small structures (e.g. the putamen) they found an underestimation of up to 50% compared to the true activity concentration. The application of the partial volume correction leads to an overestimation of about 10%, which could be considered to be a significant improvement.

Calibration

$$
\begin{aligned}
S_{Vol} &= \frac{R}{V_{VOI} \cdot c_{Vol}} \times \exp\left(\frac{T_0 - T_{cal}}{T_{1/2}} \cdot \ln 2\right) \\
&\times \left(\frac{T_{acq}}{T_{1/2}} \cdot \ln 2\right) \\
&\times \left(1 - \exp\left(-\frac{T_{acq}}{T_{1/2}} \cdot \ln 2\right)\right)^{-1}
\end{aligned} \quad (4)
$$

The calibration of the SPECT imaging system volume sensitivity S_{Vol} (e.g. in cps/Bq) (Eq. 4) is the final requirement for absolute quantitative imaging. This is

typically obtained by a correlation of the results with a calibrated well counter. The principle is briefly outlined here; details can be found in, for example, the NEMA protocols [51]: A large (to avoid partial volume effects) cylindrical phantom with known activity concentration c_{Vol} (in Bq/ml) is scanned. Corrections for attenuated and scattered photons are applied in reconstruction. A large VOI with volume V_{VOI} (in ml) is placed in the reconstructed image. T_0 is the start time, and T_{acq} the duration of the acquisition. $T_{1/2}$ is the half-time of the radionuclide used and T_{cal} the time of the activity calibration. R (in cps) represents the counting rate measured in the VOI. Finally, according to Eq. 4, a calibration factor from detected counts per second to becquerels is derived.

The calibration factor is specific for every radionuclide as well as to different intrinsic detector sensitivities and collimators used. Due to nonlinearities of the detector at different count rates and dead time effects at high activities, count rate-dependent calibration factors for the same radionuclide can sometimes be beneficial. Most notably these effects will be stronger for high-energy radionuclides; for example, Dewaraja et al. [52] have reported the effects of dead-time and pulse pile-up on quantitative SPECT with therapeutic activities (2–6 GBq) of ^{131}I.

Clinical applications

Among the applications that benefit most from absolute quantification is individualized dosimetry for planning and monitoring of therapies with internally applied radionuclides; see, for example, Geworski et al. [53]. Dewaraja et al. [54] stress the importance of SPECT dosimetry for therapy with ^{131}I-tositumomab. Sandström et al. [55] performed a dosimetric study in 24 patients treated with ^{177}Lu-DOTA-D-Phe^1-Tyr^3-octreotate with SPECT and planar imaging, and concluded that the SPECT-based method is more accurate. An extensive list of groups that apply SPECT dosimetry can be found in the review article by Flux et al. [56].

Validation studies

Many reports have shown that accurate absolute quantification is possible. The majority of the methods were evaluated in phantom or simulation studies. Recently, Shcherbinin et al. [31] reported between 3% and 5% errors in a study on a torso phantom for the isotopes ^{99m}Tc, ^{123}I, ^{131}I, and ^{111}In. Du et al. [57] achieved an error of 2% for ^{123}I in a brain phantom. In simulation studies on the MCAT cardiac torso phantom and on a ^{99m}Tc-filled torso phantom, Vandervoort et al. [32] achieved an error of 8% in the

simulation and within 4% for the phantom study. Da Silva et al. [58] reported an error of 8% in an anthropomorphic phantom with a cardiac insert for ^{99m}Tc.

Unfortunately there are only a very few reports of absolute SPECT quantification in vivo. Zeintl et al. [59] evaluated the activity of ^{99m}Tc DPD in the bladder of 16 patients. The reference activity was determined by the measurement of the activity concentration in the urine immediately after SPECT imaging. They found an average deviation of 6.8% between the activity concentration obtained in SPECT and well counter measurements, applying their version of corrections for physical effects. In another in vivo study, Da Silva et al. [45] evaluated the accuracy of absolute quantification of ^{99m}Tc-sestamibi in the myocardium of eight pigs. There was a deviation of 10% between the SPECT quantification (with their version of partial volume and attenuation correction) and the ex-vivo activity concentration of the excised myocardia. Quantification in humans has been reported by Willowson et al. [60]. They studied ^{99m}Tc-macroaggregated albumin in lung perfusion in 12 patients, and found an average error of 2.6% (ranging from −7% to +4%) with scatter, attenuation and partial volume correction. Macroaggregated albumin is thought to be trapped almost entirely in the capillaries of the lung; thus the total activity in the lung was compared to the injected activity. Almeida et al. [61] evaluated the quantitative accuracy of the striatal uptake of ^{123}I-labelled epidepride in *Papio anubis* baboons. They validated their results using PET acquisitions of ^{11}C-labelled epidepride in the same animals and found a deviation for defined ROIs of less than 10% between the two modalities using corrections for attenuation, scatter and partial volume.

Conclusion

A survey of the current literature (Fig. 5) as well as our own work shows that SPECT can be quantitative with errors of
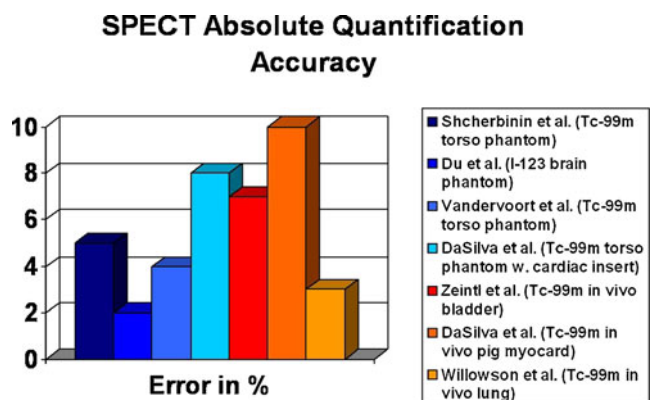

SPECT Absolute Quantification Accuracy

Legend:
- Shcherbinin et al. (Tc-99m torso phantom)
- Du et al. (I-123 brain phantom)
- Vandervoort et al. (Tc-99m torso phantom)
- DaSilva et al. (Tc-99m torso phantom w. cardiac insert)
- Zeintl et al. (Tc-99m in vivo bladder)
- DaSilva et al. (Tc-99m in vivo pig myocard)
- Willowson et al. (Tc-99m in vivo lung)

Fig. 5 Overview of the accuracy of SPECT quantification from studies reported in the literature (*blue bars* phantom studies, *red/orange bars* in vivo studies)

less than 10% even in a clinical environment. It requires careful set-up and calibration, as well as state-of-the art SPECT/CT systems and iterative reconstruction software able to accurately model the imaging physics, and to compensate for image-degrading factors (including attenuation, scatter, and partial volume).

Most of the work has been done using ^{99m}Tc tracers, and it is not clear how the absolute quantification in SPECT for other clinical set-ups (e.g. ^{99m}Tc DPD uptake in human bone, or ^{131}I uptake in the thyroid gland) could be evaluated and validated. For a variety of reasons the quantitative accuracy with high-energy radionuclides still falls behind the accuracy with low-energy radionuclides.

Nevertheless, there are also some limitations on the applicability in clinical routine. Many methods rely on complicated manual procedures. More work is needed to enable intelligent automation. In order to further reduce quantification errors, the incorporation of better imaging models in the reconstruction to allow better compensation for physical effects and patient-induced artefacts (e.g. motion) seems to be mandatory.

In general, more sophisticated phantom and animal experiments seem to be the way to go. Yet the goal of routine application of absolute quantification in clinical SPECT imaging is in the reachable range.

References

1. Bockisch A, Freudenberg LS, Schmidt D, Kuwert T. Hybrid Imaging by SPECT/CT and PET/CT: proven outcomes in cancer imaging. Semin Nucl Med. 2009;39:276–89.
2. von Schulthess GK, Steinert HC, Hany TF. Integrated PET/CT: current applications and future directions. Radiology. 2006;238:405–22. doi:10.1148/radiol.2382041977.
3. Jaszczak RJ, Greer KL, Floyd Jr CE, Harris CC, Coleman RE. Improved SPECT quantification using compensation for scattered photons. J Nucl Med. 1984;25:893–900.
4. Koral KF, Wang X, Rogers WL, Clinthorne NH, Wang X. SPECT Compton-scattering correction by analysis of energy spectra. J Nucl Med. 1988;29:195–202.
5. Frey EC, Tsui BMW. Modeling the scatter response function in inhomogeneous scattering media for SPECT. IEEE Trans Nucl Sci. 1994;41:1585–93.
6. LaCroix KJ, Tsui BMW, Hasegawa BH, Brown JK. Investigation of the use of X-ray CT images for attenuation compensation in SPECT. Nucl Sci IEEE Trans. 1994;41:2793–9.
7. Blankespoor SC, Xu X, Kaiki K, Brown JK, Tang HR, Cann CE, et al. Attenuation correction of SPECT using X-ray CT on an emission-transmission CT system: myocardial perfusion assessment. Nucl Sci IEEE Trans. 1996;43:2263–74.
8. Römer W, Reichel N, Vija HA, Nickel I, Hornegger J, Bautz W, et al. Isotropic reconstruction of SPECT data using OSEM3D: correlation with CT. Acad Radiol. 2006;13:496–502. doi:10.1016/j.acra.2005.12.004.
9. El Fakhri GN, Buvat I, Pélégrini M, Benali H, Almeida P, Bendriem B, et al. Respective roles of scatter, attenuation, depth-dependent collimator response and finite spatial resolution in

10. cardiac single-photon emission tomography quantitation: a Monte Carlo study. Eur J Nucl Med Mol Imaging. 1999;26:437–46. doi:10.1007/s002590050409.
10. Kessler RM, Ellis JRJ, Eden M. Analysis of emission tomographic scan data: limitations imposed by resolution and background. J Comput Assist Tomogr. 1984;8:514–22.
11. Geworski L, Knoop BO, de Cabrejas ML, Knapp WH, Munz DL. Recovery correction for quantitation in emission tomography: a feasibility study. Eur J Nucl Med. 2000;27:161–9.
12. Schelbert HR, Hoh CK, Royal HD, Brown M, Dahlbom MN, Dehdashti F, et al. Procedure guideline for tumor imaging using fluorine-18-FDG. J Nucl Med. 1998;39:1302–5.
13. Boellaard R. Standards for PET image acquisition and quantitative data analysis. J Nucl Med. 2009;50 Suppl 1:11S–20S. doi:10.2967/jnumed.108.057182.
14. Germain P, Baruthio J, Roul G, Dumitresco B. First-pass MRI compartmental analysis at the chronic stage of infarction: myocardial flow reserve parametric map. Comput Cardiol. 2000;2000:675–8.
15. Lewis DH, Bluestone JP, Savina M, Zoller WH, Meshberg EB, Minoshima S. Imaging cerebral activity in recovery from chronic traumatic brain injury: a preliminary report. J Neuroimaging. 2006;16:272–7. doi:10.1111/j.1552-6569.2006.00034.x.
16. Sidoti C, Agrillo U. Chronic cortical stimulation for amyotropic lateral sclerosis: a report of four consecutive operated cases after a 2-year follow-up: technical case report. Neurosurgery. 2006;58:E384. doi:10.1227/01.NEU.0000195115.30783.3A.
17. Gullberg GT, Reutter BW, Sitek A, Maltz JS, Budinger TF. Dynamic single photon emission computed tomography – basic principles and cardiac applications. Phys Med Biol. 2010;55:R111.
18. Gilland DR, Jaszczak RJ, Liang Z, Greer KL, Coleman RE. Quantitative SPECT brain imaging: effects of attenuation and detector response. Nuclear Science Symposium and Medical Imaging Conference, 1991, Conference Record of the 1991 IEEE. 1991;3:1723–27.
19. Rosenthal MS, Cullom J, Hawkins W, Moore SC, Tsui BMW, Yester M. Quantitative SPECT imaging: a review and recommendations by the Focus Committee of the Society of Nuclear Medicine Computer and Instrumentation Council. J Nucl Med. 1995;36:1489–513.
20. Tsui BM, Frey EC, Zhao X, Lalush DS, Johnston RE, McCartney WH. The importance and implementation of accurate 3D compensation methods for quantitative SPECT. Phys Med Biol. 1994;39:509–30.
21. Kohli V, King MA, Glick SJ, Pan TS. Comparison of frequency-distance relationship and Gaussian-diffusion-based methods of compensation for distance-dependent spatial resolution in SPECT imaging. Phys Med Biol. 1998;43:1025–37.
22. Kohli V, King MA, Tin-Su P, Glick SJ. Compensation for distance-dependent resolution in cardiac-perfusion SPECT: impact on uniformity of wall counts and wall thickness. Nucl Sci IEEE Trans. 1998;45:1104–10.
23. Pretorius PH, King MA, Pan TS, de Vries DJ, Glick SJ, Byrne CL. Reducing the influence of the partial volume effect on SPECT activity quantitation with 3D modelling of spatial resolution in iterative reconstruction. Phys Med Biol. 1998;43:407–20.
24. Frey EC, Tsui BM. Collimator-detector response compensation in SPECT. In: Zaidi H, editor. Quantitative analysis in nuclear medicine imaging. New York: Springer; 2005. p. 141–66.
25. Chang L-T. A method for attenuation correction in radionuclide computed tomography. Nucl Sci IEEE Trans. 1978;25:638–43.
26. Zaidi H, Hasegawa B. Determination of the attenuation map in emission tomography. J Nucl Med. 2003;44:291–315.
27. Chen J, Caputlu-Wilson S, Shi H, Galt J, Faber T, Garcia E. Automated quality control of emission-transmission misalignment for attenuation correction in myocardial perfusion imaging with

SPECT-CT systems. J Nucl Cardiol. 2006;13:43–9. doi:10.1016/j.nuclcard.2005.11.007.

28. Koral KF, Clinthorne NH, Rogers WL. Improving emission-computed-tomography quantification by Compton-scatter rejection through offset windows. Nucl Instrum Methods Phys Res Sect A. 1986;242:610–4.

29. Ogawa K, Harata Y, Ichihara T, Kubo A, Hashimoto S. A practical method for position-dependent Compton-scatter correction in single photon emission CT. Med Imaging IEEE Trans. 1991;10:408–12.

30. Zaidi H, Koral K. Scatter correction strategies in emission tomography. In: Zaidi H, editor. Quantitative analysis in nuclear medicine imaging. New York: Springer; 2006. p. 205–35.

31. Shcherbinin S, Celler A, Belhocine T, Vanderwerf R, Driedger A. Accuracy of quantitative reconstructions in SPECT/CT imaging. Phys Med Biol. 2008;53:4595–604.

32. Vandervoort E, Celler A, Harrop R. Implementation of an iterative scatter correction, the influence of attenuation map quality and their effect on absolute quantitation in SPECT. Phys Med Biol. 2007;52:1527–45.

33. Wells RG, Celler A, Harrop R. Analytical calculation of photon distributions in SPECT projections. Nucl Sci IEEE Trans. 1998;45:3202–14.

34. Floyd CE, Jaszczak RJ, Harris CC, Coleman RE. Energy and spatial distribution of multiple order Compton scatter in SPECT: a Monte Carlo investigation. Phys Med Biol. 1984;29:1217–30.

35. Ljungberg M, Strand S-E. Scatter and attenuation correction in SPECT using density maps and Monte Carlo simulated scatter functions. J Nucl Med. 1990;31:1560–7.

36. Frey EC, Tsui BM. Parameterization of the scatter response function in SPECT imaging using Monte Carlo simulation. Nucl Sci IEEE Trans. 1990;37:1308–15.

37. Cherry SR, Sorenson JA, Phelps ME. Physics in nuclear medicine. 3rd ed. Philadelphia: Elsevier; 2003.

38. Schramm NU, Ebel G, Engeland U, Schurrat T, Behe M, Behr TM. High-resolution SPECT using multipinhole collimation. Nucl Sci IEEE Trans. 2003;50:315–20.

39. Branderhorst W, Vastenhouw B, van der Have F, Blezer E, Bleeker W, Beekman F. Targeted multi-pinhole SPECT. Eur J Nucl Med Mol Imaging. 2011;38:552–561.

40. Hoffman EJ, Huang S-C, Phelps ME. Quantitation in positron emission computed tomography: 1. Effect of object size. J Comput Assist Tomogr. 1979;3:299–308.

41. Chen CH, Muzic Jr RF, Nelson AD, Adler LP. A nonlinear spatially variant object-dependent system model for prediction of partial volume effects and scatter in PET. Med Imaging IEEE Trans. 1998;17:214–27.

42. Seo Y, Aparici CM, Cooperberg MR, Konety BR, Hawkins RA. In vivo tumor grading of prostate cancer using quantitative 111In-capromab pendetide SPECT/CT. J Nucl Med. 2009;51:31–6. doi:10.2967/jnumed.109.067108.

43. Hutton BF, Lau YH. Application of distance-dependent resolution compensation and post-reconstruction filtering for myocardial SPECT. Phys Med Biol. 1998;43:1679–93.

44. Pretorius PH, King MA. Diminishing the impact of the partial volume effect in cardiac SPECT perfusion imaging. Med Phys. 2009;36:105–15.

45. Da Silva AJ, Tang HR, Wong KH, Wu MC, Dae MW, Hasegawa BH. Absolute quantification of regional myocardial uptake of 99mTc-Sestamibi with SPECT: experimental validation in a porcine model. J Nucl Med. 2001;42:772–9.

46. Tang HR, Brown JK, Hasegawa BH. Use of X-ray CT-defined regions of interest for the determination of SPECT recovery coefficients. Nuclear Science Symposium, 1996 Conference Record, 1996 IEEE. 1996;3:1840–44.

47. Rousset O, Ma Y, Kamber M, Evans AC. 3D simulations of radiotracer uptake in deep nuclei of human brain. Comput Med Imaging Graph. 1993;17:373–9.

48. Rousset OG, Ma Y, Evans AC. Correction for partial volume effects in PET: principle and validation. J Nucl Med. 1998;39:904–11.

49. Du Y, Tsui BM, Frey EC. Partial volume effect compensation for quantitative brain SPECT imaging. Med Imaging IEEE Trans. 2005;24:969–76.

50. Soret M, Koulibaly PM, Darcourt J, Hapdey S, Buvat I. Quantitative accuracy of dopaminergic neurotransmission imaging with 123I SPECT. J Nucl Med. 2003;44:1184–93.

51. National Electrical Manufacturers Association. Performance measurements of gamma cameras. NEMA NU 1–2007. Rosslyn, VA: National Electrical Manufacturers Association. 2007.

52. Dewaraja Y, Ljungberg M, Koral K. Effects of dead time and pile up on quantitative SPECT for I-131 dosimetric studies. J Nucl Med. 2008;49(Suppl 1):47P.

53. Geworski L, Schaefer A, Knoop BO, Pinkert J, Plotkin M, Kirsch CM. Physikalische Aspekte szintigraphisch basierter Dosimetrie bei nuklearmedizinischen Therapien. Nuklearmedizin. 2010;49:79–123.

54. Dewaraja YK, Schipper MJ, Roberson PL, Wilderman SJ, Amro H, Regan DD, et al. 131I-Tositumomab radioimmunotherapy: initial tumor dose-response results using 3-dimensional dosimetry including radiobiologic modeling. J Nucl Med. 2010;51:1155–62. doi:10.2967/jnumed.110.075176.

55. Sandström M, Garske U, Granberg D, Sundin A, Lundqvist H. Individualized dosimetry in patients undergoing therapy with (177)Lu-DOTA-D-Phe (1)-Tyr (3)-octreotate. Eur J Nucl Med Mol Imaging. 2010;37:212–25. doi:10.1007/s00259-009-1216-8.

56. Flux G, Bardies M, Monsieurs M, Savolainen S, Strands SE, Lassmann M. The impact of PET and SPECT on dosimetry for targeted radionuclide therapy. Z Med Phys. 2006;16:47–59.

57. Du Y, Tsui BM, Frey EC. Model-based compensation for quantitative 123I brain SPECT imaging. Phys Med Biol. 2006;51:1269–82.

58. Da Silva AJ, Tang HR, Wu MC, Hasegawa BH. Absolute quantitation of myocardial activity in phantoms. Nucl Sci IEEE Trans. 1999;46:659–66.

59. Zeintl J, Vija AH, Yahil A, Hornegger J, Kuwert T. Quantitative accuracy of clinical 99mTc SPECT/CT using ordered-subset expectation maximization with 3-dimensional resolution recovery, attenuation, and scatter correction. J Nucl Med. 2010;51:921–8. doi:10.2967/jnumed.109.071571.

60. Willowson K, Bailey DL, Baldock C. Quantitative SPECT reconstruction using CT-derived corrections. Phys Med Biol. 2008;53:3099–112.

61. Almeida P, Ribeiro MJ, Bottlaender M, Loc'h C, Langer O, Strul D, et al. Absolute quantitation of iodine-123 epipride kinetics using single-photon emission tomography: comparison with carbon-11 epipride and positron emission tomography. Eur J Nucl Med Mol Imaging. 1999;26:1580–8. doi:10.1007/s002590050498.